NATURAL FREQUENCIES ESTIMATION OF A MONOPILE SUPPORTED DTU-10MW OFFSHORE WIND TURBINE

Philip Alkhoury, University of Nantes, France, Philip.alkhoury@etu.univ-nantes.fr
Abdul-Hamid Soubra, University of Nantes, France, Abed.Soubra@univ-nantes.fr
Valentine Rey, University of Nantes, France, Valentine.rey@univ-nantes.fr
Mourad Aït-Ahmed, University of Nantes, France, Mourad.ait-ahmed@univ-nantes.fr

ABSTRACT

The design of an offshore wind turbine (OWT) founded on a monopile foundation is principally based on a dimensioning criteria related to its fundamental frequencies. These frequencies must remain outside the excitation frequencies to avoid resonance. For the calculation of the OWT natural frequencies, several studies exist but few of them simultaneously consider both the real geometrical configuration of the OWT superstructure (tower, blades, transition piece and nacelle) and the three-dimensional (3D) soil domain and its interaction with the monopile foundation. In order to ensure accurate determination of the system frequency, a full 3D model of a 10 MW DTU offshore wind turbine installed in sand is developed and simulated using the commercially available finite element code ABAQUS/Standard. The main objective is to perform a rigorous modal analysis of the wind turbine considering the entire soil-foundation-structure system. The obtained natural frequencies are compared with those corresponding to other simplified foundation models. In addition, the effect of (i) the monopile diameter and embedded depth and (ii) the sand relative density, on the system natural frequency is presented. Results indicate that when considering the soil-structure interaction the OWT's first natural frequency is substantially decreased. Nonetheless, among the numerous foundation models found in literature, the distributed spring model based on the modulus of subgrade reaction proved to give the best estimate in terms of the first natural frequency. Finally, results have shown that there exists a critical monopile embedded depth above it there is no further increase in the first natural frequency.

Keywords: natural frequency, soil-structure interaction, foundation models, monopile

INTRODUCTION

During their lifetime, OWTs are exposed to intense dynamic loading in a wide frequency range, which makes them dynamically sensitive structures. Therefore, tuning the natural frequencies of the whole structure is of special importance during the design stage. Indeed, the first natural frequency of the overall wind turbine should be carefully adjusted in a very narrow range to be outside the excitation frequencies and thus to avoid resonance.

The excitation loads on offshore wind turbines are (i) the environmental loading from wind turbulence and ocean waves and (ii) the mechanical loadings coming from both the rotational speed of the rotor (often denoted by $1P$ frequency band) and the shadowing effect caused by the blades passage in front of the tower (termed as N_bP frequency band, where N_b is the number of blades). Depending on the natural frequency of the OWT structure, three design options are possible: soft-soft, soft-stiff and stiff-stiff. Among these, soft-stiff is the preferred design option in which the natural frequency is designed to be between the $1P$ and $3P$ frequency bands.

Accurate estimates of the natural frequency of an OWT are essential for an effective design. Realistic models of both the OWT structural components and the foundation are thus necessary to accurately compute the natural frequencies. Usually, the OWT superstructure is merely modeled by a beam representing the tower with a lumped mass at its top to represent the nacelle and the blades (Adhikari and Bhattacharya 2011; Andersen et al. 2012; Bisoi and Haldar 2014; Arany et al. 2016). Furthermore, the soil-structure interaction is sometimes

modelled using a simplified approach by assuming a fixed base (rigid soil). This assumption could lead up to 20% of errors in natural frequencies of the structure (cf. DNV 2002), which can be unacceptable with regard to resonance risk assessment. Other approaches attempt to include the soil flexibility in their models. In this regard, the soil-foundation system is modelled using the well-known Winkler approach in which the monopile is represented by an elastic beam and the soil is substituted by equivalent springs distributed along the monopile embedded depth. Within this approach, the springs' stiffness is usually determined by the so-called p-y curves recommended by the API (2011). Note that the API-based p-y curves were initially designed for slender flexible piles which are widely used for offshore oil and gas applications. They may not be applicable to large diameter monopiles used as supports for OWTs. In addition to the Winkler approach, the coupled stiffness matrix is also used by many investigators to estimate the OWT natural frequency (cf. Adhikari and Bhattacharya 2011; Arany et al. 2016). In this model, the monopile-soil system is replaced by coupled translational and rotational springs at the mudline.

This paper aims to calculate the natural frequency of an OWT using a 3D model. This model simultaneously considers (i) the geometrical and mechanical properties of the OWT superstructure (tower, blades, transition piece and nacelle) and (ii) the 3D soil domain to better describe its interaction with the monopile foundation. The results are compared with those obtained from other simplified foundation models. Finally, the effect of the monopile embedded depth and diameter on the OWT natural frequency is investigated for two cases of loose and very dense sands.

MECHANICAL MODEL OF THE DTU 10 MW WIND TURBINE

The modern DTU 10 MW three-bladed wind turbine is selected as an example in the present study because it is a representative of utility-scale OWT being manufactured today. Figure 1 provides a schematic diagram of the full structure with the relevant dimensions. Its properties are well defined in many previous studies (cf. Bak et al. 2013). Table 1 provides the properties of the DTU 10 MW used in this work. The total length of the monopile is chosen as 80 m, in which 25 m and 45 m are in the water and seabed respectively and another 10 m is added above the mean sea level corresponding to the transition piece. The diameter of the monopile foundation was taken the same as the one of the bottom cross-section of the tower. A constant monopile thickness throughout the length of the monopile of 0.09 m is chosen respecting the minimum wall thickness recommended by API (cf. API 2000). It should be noted that the turbine tower is divided into ten sections with decreasing diameter and thickness from bottom to top where the wall thickness is constant within each section (cf. Bak et al. 2013). Table 2 gives the diameter and wall thickness distribution of the tower along its height.

Table 1. Properties of the DTU 10 MW wind turbine

Blade	Rotor diameter	178.332 m
	Cut-in, Rated rotor speed	6 rpm, 9.6 rpm
	Length	86.366 m
	Overall mass	41,716 kg
Hub and Nacelle	Hub diameter, hub height	5.6 m, 119 m
	Hub mass	105,520 kg
	Nacelle mass	446,036 kg
Tower	Height above transition piece	115.63 m
	Mass	682, 442 kg
	Top diameter, bottom diameter	5.5 m , 8.3 m
	Top wall thickness, bottom wall thickness	0.02 m, 0.038 m

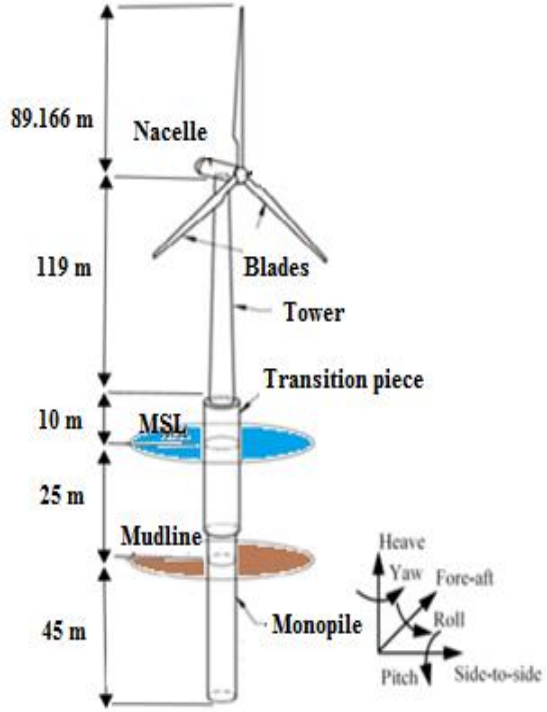

Fig. 1. DTU 10 MW model (Front View)

Table 2. Wall thickness distribution of the tower

Height [m]	Outer diameter [m]	Wall thickness [mm]
0 11.5	8.3 8.0215	38
11.501 23	8.0215 7.7431	36
23.001 34.5	7.7431 7.4646	34
34.501 46	7.4646 7.1861	32
46.001 57.5	7.1861 6.9076	30
57.501 69	6.9076 6.6292	28
69.001 80.5	6.6292 6.3507	26
80.501 92	6.3507 6.0722	24
92.001 103.5	6.0722 5.7937	22
103.501 115.63	5.7937 5.5	20

Development of the 3D model of the wind turbine

The 3D model of the DTU 10 MW wind turbine is developed using the finite element code ABAQUS/Standard. The ten sections of the tower as well as the 10 m transition piece are modelled using shell elements (S8R). The monopile (in contact with water and with the soil) is modeled using solid elements (C3D8R) to conveniently consider the soil-structure interaction. The different parts of the tower as well as, the tower and transition piece, and the transition piece and monopile, are tied with each other at their adjacent cross-sections. Each blade is partitioned into a number of segments (51) along its length. A generalized beam cross section in ABAQUS is defined for every segment, where each cross section is assigned stiffness and mass properties that can be found in Bak et al. (2013). Only the masses and rotary inertia of the nacelle/hub assembly are considered in the 3D model; they are modelled by a point mass element lumped at the top of the tower. A hinge connection between the tower and the blades is defined to consider the blades rotation with respect to the turbine rotor.

Table 3 provides the material properties of the tower, transition piece and monopile. It should be noted that the density of the monopile in water is slightly larger than that of the tower since the interaction between the monopile and the surrounding water is considered by the additional mass in the 3D model (cf. Zuo et al. 2018). Figure 2 shows the developed 3D model of the wind turbine superstructure (tower, nacelle/hub and blades).

Table 3. Material properties of the wind turbine

Component	Material	Density (kg/m3)	Young modulus (GPa)	Poisson ratio
Tower and transition piece	Steel	8500	210	0.3
Monopile in the water	Steel	8880	210	0.3
Monopile in the soil	Steel	7850	210	0.3

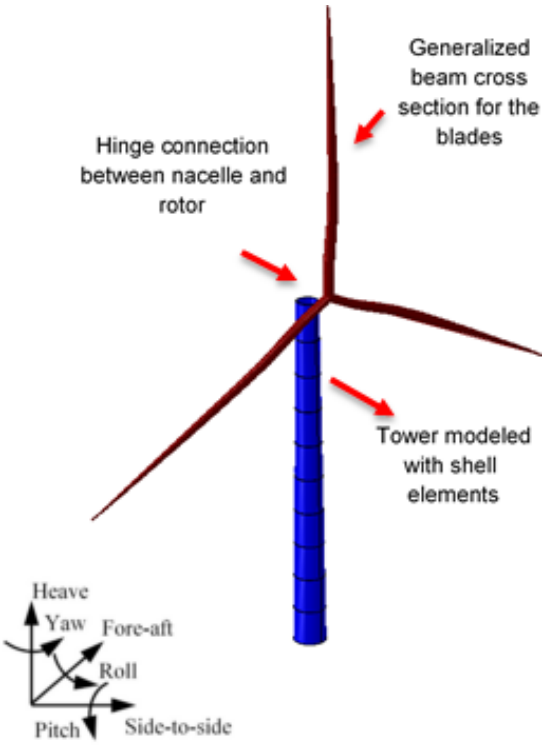

Fig. 2. 3D model of the wind turbine superstructure

The soil-monopile interaction is modelled by considering the soil surrounding the monopile as a 3D continuum. The soil around and inside the monopile is modelled by a weightless linear elastic material using 8-noded brick elements with reduced integration (C3D8R). Results of a convergence test have shown that a 20D diameter and 1.7L height can be adopted for the 3D soil domain, where D and L are the monopile outer diameter and embedded depth respectively. The bottom of the soil model is fixed in all directions, whereas the lateral boundary is restrained in the horizontal directions. The interaction between the monopile and the soil is simulated using small sliding, surface-to-surface master/slave contact pair formulation.

In the present work, a depth-dependent small strain Young's modulus profile based on cone penetration tests (CPT) data is adopted for the sandy soil. Synthetic CPT profiles derived by Lunne and Christopherson (1983) and used by Prendergast et al. (2015) are employed herein to derive the depth-dependent cone tip resistance q_c values for different sand relative densities as follows:

$$q_c = 60(\sigma_v')^{0.7}\exp(2.91D_r) \quad [1]$$

where, D_r is the relative density of sand , σ_v' is the vertical effective stress (kPa). The small strain shear modulus G_0 profiles are then derived from the synthetic q_c values using the equation given by Jardine et al. (2005) as follows:

$$G_0 = q_c[A + B\eta - C\eta^2]^{-1} \quad [2]$$

where $A = 0.0203$, $B = 0.00125$, $C = 1.216E-6$ and $\eta = q_c(P_a\sigma_v')^{-0.5}$; P_a is a reference pressure of $100\ kPa$ (atmospheric pressure). The derived G_0 profiles were then converted to a profile of the small strain Young's modulus E_0 using the following formula:

$$E_0 = 2G_0(1 + \nu_0) \quad [3]$$

where the small strain Poisson's ratio ν_0 is derived from the G_0 profile by using the equation

derived by Gu et al. (2013) as follows:

$$\nu_0 = 0.62(G_0)^{-0.2} \quad [4]$$

Figure 3-a and Figure. 3-b, show respectively the derived synthetic cone tip resistance (q_c) profile and the corresponding small-strain Young's modulus (E_0) profile in the cases of a loose and a very dense sand having respectively a relative density of 30% and 80% and a bulk unit weight of $16\ kN/m^3$ and $20\ kN/m^3$.

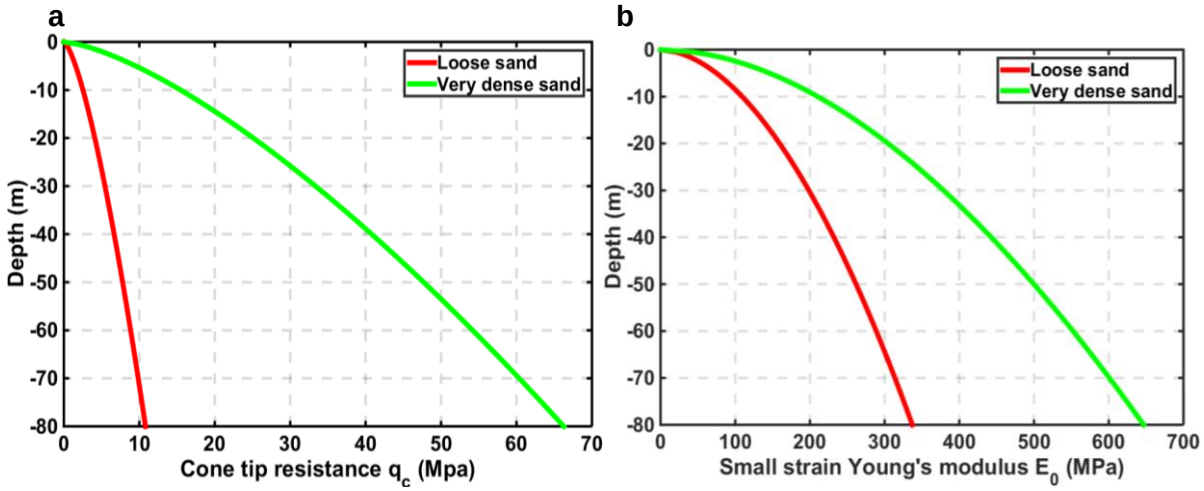

Fig. 3. Synthetic profiles for loose and very dense sands (a) cone tip resistance q_c and (b) small strain Young's modulus E_0

NUMERICAL RESULTS

Firstly, the natural frequencies and the corresponding vibration modes of the 10 MW DTU OWT installed in loose sand are presented and discussed. Secondly, the obtained natural frequencies from the developed 3D model are compared with those calculated by adopting the different alternative simplified foundation models presented above (i.e. the fixed base model, the coupled spring stiffness matrix model and the distributed springs' model). Finally, the effect of the monopile embedded length on the system natural frequency is investigated for two different monopile diameters and for two sand relative densities.

Numerical results of the developed 3D model

Table 4 and Figure 4 provide the natural frequencies and the corresponding vibration modes of the wind turbine as obtained from a modal analysis in ABAQUS. The modal analysis shows that the major mode shapes of a monopile supported OWTs are the first bending modes of the tower in the side-to-side and the fore-aft directions as shown in Table 4 and Figure 4. The natural frequencies of these two modes are slightly different because the moment of inertia of rotor-nacelle assembly in the roll motion is different from that corresponding to the pitch motion. Notice, however that the difference is very small because the tower and foundation have axial symmetric shapes and properties. The subsequent mode shapes are those of the blade (Modes 3, 4, 5, 6, 7, 9, 11 and 12) and the second bending modes of the tower (Modes 8 and 10).

Table 4. Natural frequencies of the monopile supported 10 MW DTU wind turbine in sand

Mode	Description	Frequency (Hz)
1	1st Bending tower, side-side	0.201
2	1st Bending tower, fore-aft	0.203
3	1st Blade asymmetric, flapwise yaw	0.566
4	1st Blade asymmetric, flapwise tilt	0.598
5	1st Blade collective flap	0.761
6	1st Blade asymmetric, edgewise 1	0.904
7	1st Blade asymmetric, edgewise 2	0.913
8	2nd Bending tower, fore-aft	1.282
9	2nd Blade asymmetric, flapwise Yaw	1.364
10	2nd Bending tower, side-side	1.445
11	2nd Blade collective flap	1.634
12	2nd Blade asymmetric, flapwise tilt	1.690

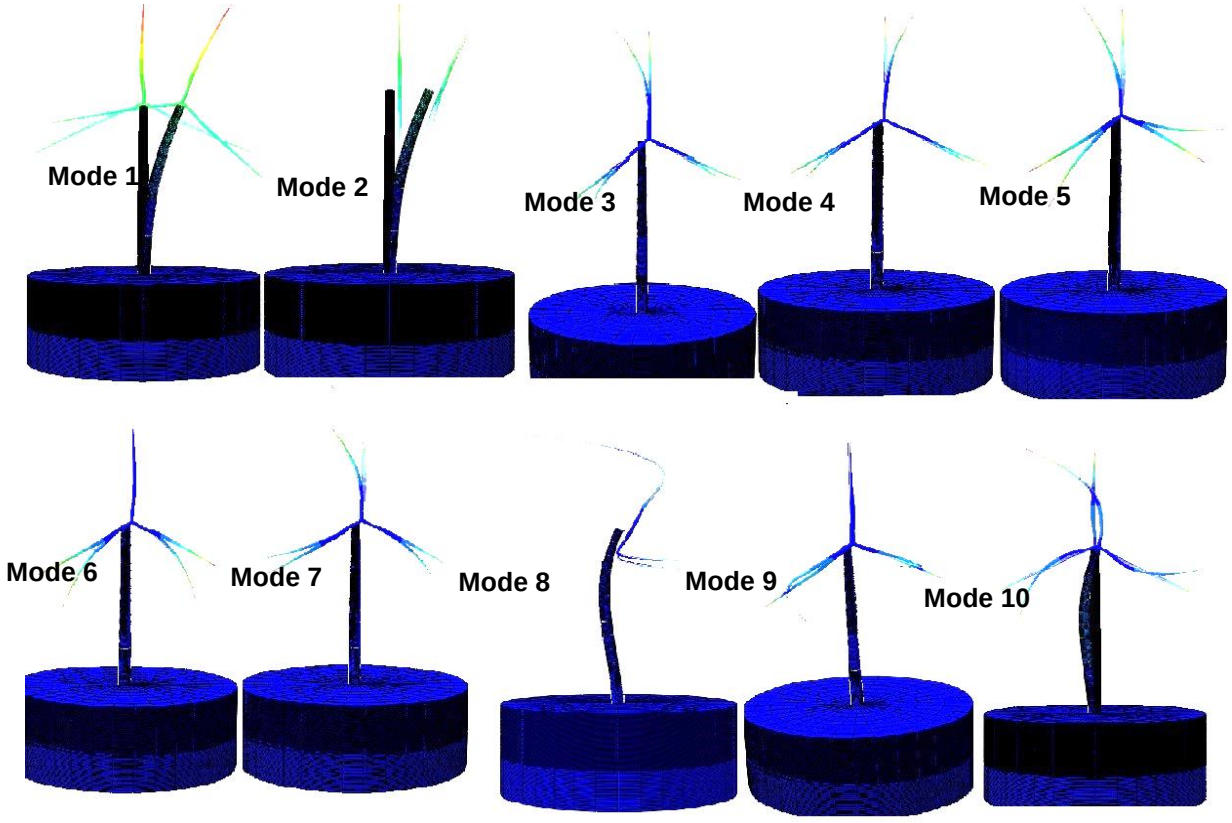

Fig. 4. Vibration modes of the wind turbine

Comparison with other foundation models

The different simplified foundation models considered in this study for the sake of comparison are the fixed-base model, the coupled springs model and the distributed springs model. They are illustrated in Figure 5 and are discussed below.

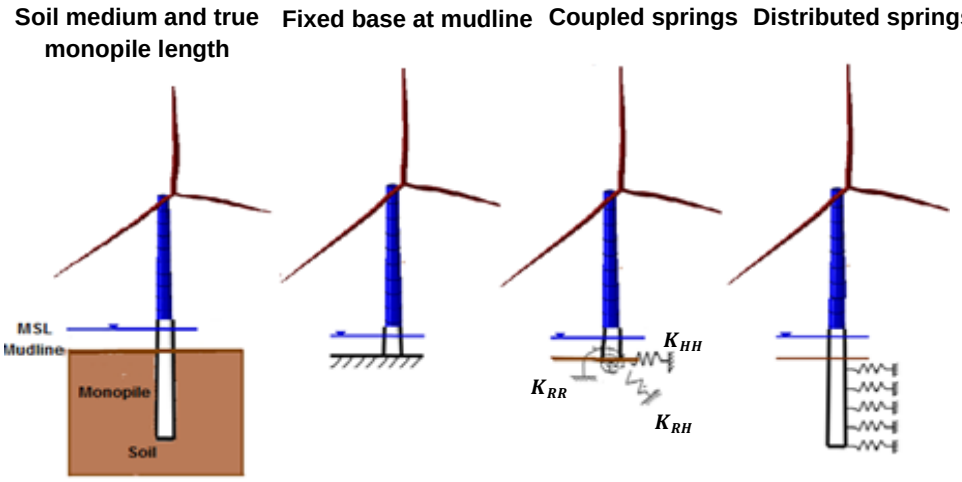

Fig. 5. Alternative simplified foundation models analyzed in this paper

- The fixed base model ignores completely the soil flexibility and assumes a perfect rigid connection at seabed.

- The coupled spring model considers the soil flexibility. In this model, the soil and the embedded monopile are replaced by linear elastic coupled translational and rotational springs (K_{HH}, K_{RR}, K_{RH}) placed at the mudline as shown in Figure 5. Several analytical expressions can be found in literature for obtaining the stiffness of the coupled translational and rotational springs in the case of a rigid monopile. Table 5 below summarizes the expressions that are used in this study to calculate the stiffness matrix at mudline. These expressions are those corresponding to a linear or a parabolic soil profile to capture the depth-dependent Young modulus considered in Figure 3-b.

Table 5. Expressions used in this work for the coupled spring stiffnesses

Authors	Soil model	$\boldsymbol{K_{HH}}$	$\boldsymbol{K_{RR}}$	$\boldsymbol{K_{RH}}$
Poulos and Davis (1980)	Linear[a]	$\frac{1}{2}L^2.n_h$	$\frac{1}{4}L^4.n_h$	$-\frac{1}{3}L^3.n_h$
Huggins and Basu (2011)	Linear[b, c]	$\frac{4E_s.r}{f(\nu)}.(\frac{L}{D})^{1.66}$	$\frac{15.4E_s.r^3}{f(\nu)}.(\frac{L}{D})^{3.45}$	$-\frac{6.7E_s.r^2}{f(\nu)}.(\frac{L}{D})^{2.66}$
Shadlou and Battacharya (2016)	Parabolic[b, c]	$5.33E_s.r.f(\nu).(\frac{L}{D})^{1.07}$	$13E_s.r^3.f(\nu).(\frac{L}{D})^{3}$	$-7.2E_s.r^2.f(\nu).(\frac{L}{D})^{2}$

[a] The coefficient of subgrade reaction n_h for sand is given as $n_h = \frac{A.\gamma_{sand}}{1.35}$ where γ_{sand} is the specific weight of sand and A=100-300 for loose sand

[b] $f(\nu) = \frac{1+\nu}{1+0.75\nu}$

[c] E_s is the soil Young modulus at a depth equal to the pile diameter. L, r and D are the monopile embedded length, radius and outer diameter respectively.

- The distributed springs' model replaces the soil with a series of discrete and independent linear springs distributed along the true embedded depth of the monopile length. The stiffness of the distributed springs can be determined based on many different methods. In this study and for the sake of comparison, three different approaches are adopted to determine the stiffness of the springs:
  - (i) the approach based on the modulus of subgrade reaction using the modified expression derived by Vesic (1961);
  - (ii) the p-y curves derived from CPT q_c - values given by Suryasentana and Lehane (2014);
  - (iii) the API based $p-y$ curves for piles in sand recommended by the API code.

It should be noted that the fundamental frequency of the OWT system is determined within these approaches using linear Eigen-frequency analysis in ABAQUS by considering only the initial stiffness (initial slope) of the $p-y$ curves. Figure 6 shows the discrete spring stiffness distribution along the monopile embedded length (45 m) as given by the three different approaches. A total of 45 springs equally-spaced at 1.0m interval are used in the analysis.

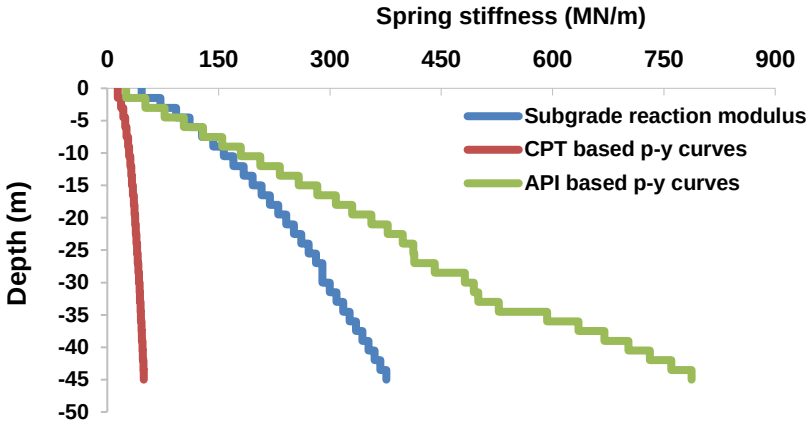

Fig. 6. Spring stiffness distribution along the monopile embedded depth

For each one of the seven foundation models presented above, the natural frequencies and the corresponding vibration modes are determined by performing a modal analysis on ABAQUS. For conciseness, only the first natural frequency is reported herein. Figure 7 shows a comparison between the first natural frequency obtained from the different foundation models and the one obtained by the present 3D model.

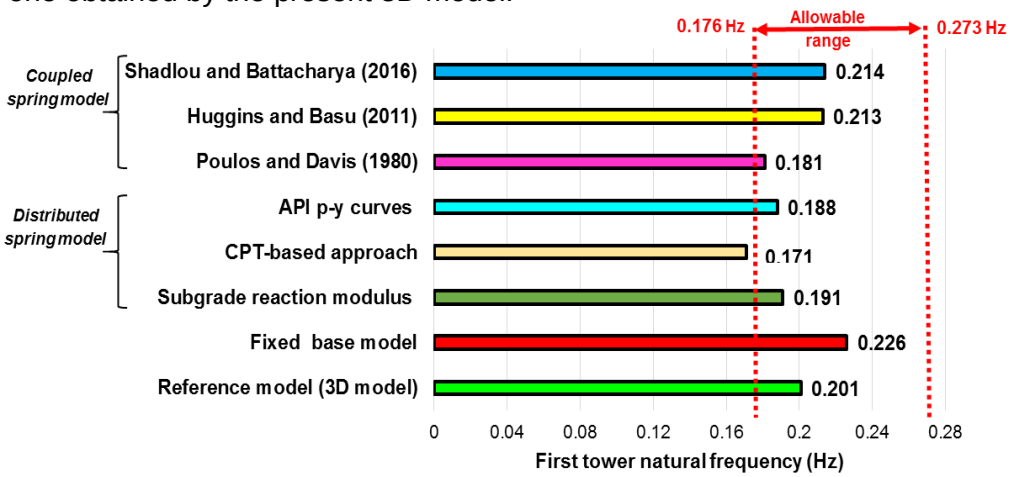

Fig. 7. Predicted first natural frequency for the several foundation models

From Figure 7, one may observe that almost all of the foundation models considered in this study give an estimation of the first natural frequency which lies within the allowable frequency range of the 10 MW DTU OWT (i.e. 0.176 Hz – 0.273 Hz) except the distributed spring model where the spring stiffness is calculated based on CPT data.

Table 6 gives the percentage error between the first natural frequency corresponding to the different foundation models and that calculated using the developed 3D model. The CPT-based approach proves to underestimate the natural frequency by about 14.9% compared to the 3D model. On the contrary, the fixed base model overestimates the value of the frequency by around 12.4%. This overestimation is expected; the soil flexibility being neglected within this approach.

Concerning the coupled spring models, the expressions given Poulos and Davis (1980) underestimate the value of the natural frequency by 10%. However, both Huggins and Basu (2011) and Shadlou and Battacharya (2016) overestimate this frequency by about 6% and 6.5% respectively. The values of the natural frequency calculated by Huggins and Basu (2011) and Shadlou and Bhattacharya (2016) are close to that provided by the fixed base model, thus overestimating the foundation stiffness.

Notice finally that the distributed spring stiffness model based on the API $p-y$ curves and the one based on the modulus of subgrade reaction underestimate the natural frequency with a relatively acceptable error of 6.5% and 5% respectively.

Table 6. Relative error between the first natural frequency estimated using the 3D model and the ones estimated using the existing foundation models

	Different Foundation Models	***1st Natural frequency (Hz)***	***Error (%)***
	3D model (Reference model)	0.201	-
	Fixed Base model	0.226	12.4
Distributed springs model	Subgrade reaction modulus	0.191	-5
	CPT-based approach	0.171	-14.9
	API p-y curves	0.188	-6.5
Coupled springs model	Poulos and Davis (1980)	0.181	-10
	Huggins and Basu (2011)	0.213	6
	Shadlou and Battacharya (2016)	0.214	6.5

Impact of the monopile embedded depth

Figure 8 illustrates the effect of varying the monopile embedment depth (from 1D to 12D) on the first natural frequency of the DTU 10 MW OWT for two monopile diameters D (D = 8.3 m and 10 m) and for two sand types (loose and very dense sands) making use of the 3D developed model.

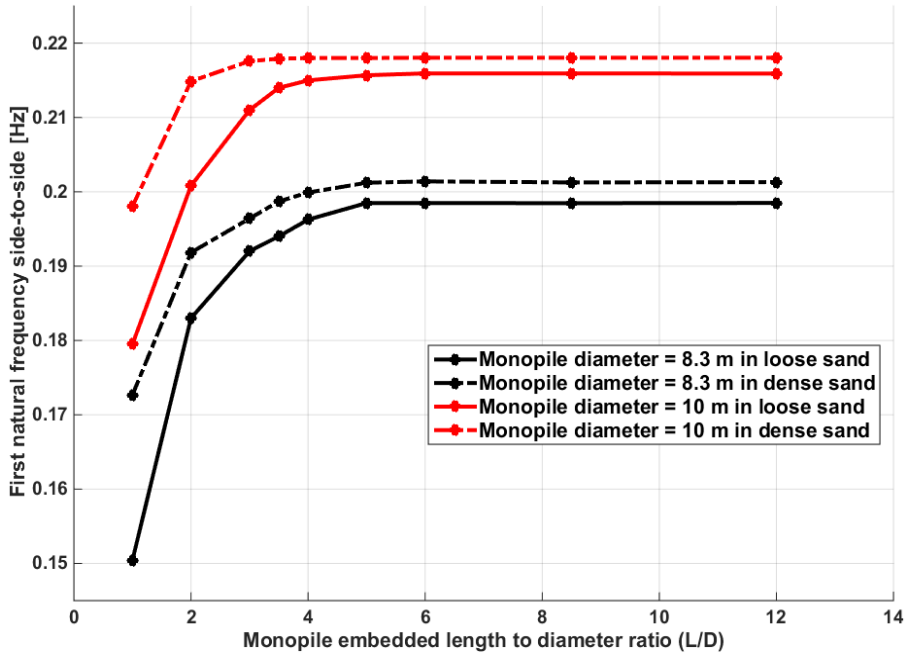

Fig. 8. First natural frequency versus the monopile embedded length

From Figure 8, one may observe that increasing the embedment depth from 5D to 12D has no significant influence on the overall natural frequency of the OWT having a designed pile diameter of 8.3 m and installed in loose sand. A decrease in the embedment depth below 5D significantly decreases the natural frequency. For the same monopile diameter installed in very dense sand, a similar behavior may also be observed. Moreover, when increasing the monopile diameter to 10 m, it can be seen that no further increase in the natural frequency is observed starting from a much lower monopile embedded depth of around 4D when installed in loose sand and 3.5D when installed in very dense sand. Notice also that the increase in the monopile diameter is shown to induce a significant increase in the value of the natural frequency. For instance, the natural frequency increases by about 9.1% in the case of a loose sand when the monopile diameter increases from 8.3 m to 10 m.

CONCLUSIONS

In this paper, a 3D model considering the whole OWT superstructure and the 3D soil domain together with its interaction with the foundation is developed. The aim is to accurately compute the natural frequencies of the 10 MW DTU OWT installed in sand. The obtained results are compared with those corresponding to some alternative simplified foundation models found in literature. Also, the influence of the monopile embedded depth and diameter and the sand relative density on the natural frequency was investigated. Based on the obtained numerical results, the following conclusions can be drawn:

1. The first bending modes of the tower in the side-to-side and the fore-aft directions are the major mode shapes of a monopile supported OWT;
2. The first vibration frequency of the tower is significantly decreased (by 12.4 %) when the soil-structure interaction is considered;
3. Among the different foundation models found in literature, the distributed spring model based on the modulus of subgrade reaction proved to give the best estimate in terms of the first natural frequency with a relative error of around 5%. This result is in conformity with the finding by Ashford and Juirnarongrit (2003) who concluded that models employing the modified expression of Vesic (1961) for the modulus of subgrade reaction are capable of estimating the natural frequencies within a ratio of 0.98-1.04 times the measured experimental values;
4. The natural frequency of the OWT increases with an increase in the monopile embedded length, and then it becomes constant beyond a critical embedded depth. The limit value of the embedded depth decreases with the increase in the monopile diameter and the increase of the sand relative density. The finding related to the critical embedded depth is important in design in order to avoid unnecessary over length of the monopile embedded depth.

ACKNOWLEDGMENTS

This work is carried out within the framework of the WEAMEC, West Atlantic Marine Energy Community, and the funding from the CARENE, Communauté d' Agglomération de la Région Nazairienne et de l'Estuaire.

REFERENCES

Adhikari, S., and Bhattacharya, S., 2011. Vibrations of wind-turbines considering soil-structure interaction. Wind and Structures*, 14*(2) 85–112.

American Petroleum Institute (API), 2011. Petroleum and natural gas industries - specific requirement for offshore structures. *Part 4* - Geotechnical and Foundation Design Considerations.

Andersen, L. V., Vahdatirad, M. J., Sichani, M. T., and Sørensen, J. D., 2012. Natural frequencies of wind turbines on monopile foundations in clayey soils - A probabilistic approach. Computers and Geotechnics, *43* 1–11.

API, 2000. Recommended Practice for Planning, Designing and Construction Fixed Offshore Platforms - working Stress Design. *API RP2A-WSD*.

Arany, L., Bhattacharya, S., Macdonald, J. H. G., and Hogan, S. J., 2016. Closed form solution of Eigen frequency of monopile supported offshore wind turbines in deeper waters incorporating stiffness of substructure and SSI. Soil Dynamics and Earthquake Engineering, *83* 18–32.

Ashford, S., and Juirnarongrit, T., 2003. Evaluation of pile diameter effect on initial modulus of subgrade reaction. Journal of Geotechnical and Geoenvironmental Engineering, *129* 234–242.

Bak, C., Zahle, F., Bitsche, R., Yde, A., Henriksen, L. C., Nata, A., and Hansen, M. H., 2013. Description of the DTU 10 MW Reference Wind Turbine. DTU Wind Energy, Report-I-0092, 138p.

Bisoi, S., and Haldar, S., 2014. Dynamic analysis of offshore wind turbine in clay considering soil-monopile-tower interaction. Soil Dynamics and Earthquake Engineering, *63* 19–35.

Gu, X., Yang, J., and Huang, M., 2013. Laboratory measurements of small strain properties of dry sands by bender element. Soils and Foundations, *53*(5) 735–745.

Higgins, W., and Basu, D., 2011. Fourier finite element analysis of laterally loaded piles in elastic media. Storrs, Connecticut, US.

Jardine, R.J., Chow, F.C., Overy, R.F., and Standing, J., 2005. ICP design methods for driven piles in sands and clays, London.

Lunne, T., and Christopherson, H.P, 1983. Interpenetration of cone penetrometer data for offshore sands. Proceedings of the Offshore Technology Conference OTC4464. Houston, Texas.

Poulos H, and Davis E, 1980. Pile foundation analysis and design. New York: Rainbow-Bridge Book Co., Wiley.

Prendergast, L. J., Gavin, K., and Doherty, P., 2015. An investigation into the effect of scour on the natural frequency of an offshore wind turbine. Ocean Engineering, 101 1–11.

Shadlou, M., and Bhattacharya, S., 2016. Dynamic stiffness of monopiles supporting offshore wind turbine generators. Soil Dynamics and Earthquake Engineering, 88 15–32.

Suryasentana, S., and Lehane, B., 2014. Numerical derivation of CPT-based p-y curves for piles in sand. Géotechnique, *64*(3) 186–194.

DNV Veritas, N., 2002. Guidlines for design of wind turbines, Det Norske Veritas: Wind Energy Department, Ris National Laboratory.

Vesic, A., 1961. Bending of beams resting on isotropic elastic solid. Journal of the Soil Mechanics and Foundations Division, 87 35–53.

Zuo, H., Bi, K., and Hao, H., 2018. Dynamic analyses of operating offshore wind turbines including soil-structure interaction. Engineering Structures, 157 42–62.